Springer

KSME

Journal of Mechanical Science and Technology 26 (5) (2012) 1471~1476
www.springerlink.com/content/1738-494x
DOI 10.1007/s12206-012-0342-6

Research on corrosion behavior of A6N01S-T5 aluminum alloy welded joint for high-speed trains †

Guoqing Gou[1], Nan Huang[1,*], Hui Chen[1], Hongmei Liu[1], Aiqin Tian[2] and Zhicheng Guo[2]

[1]*School of Material Science and Engineering, Southwest Jiaotong University, Chengdu, 610031, China*
[2]*CSR Qingdao Sifang Co., Ltd, Qingdao, 266000, China*

(Manuscript Received March 23, 2011; Revised October 28, 2011; Accepted February 1, 2012)

Abstract

For high speed trains, safety is of utmost importance. Salt fog corrosion, intergranular corrosion tests were employed to observe the corrosion behavior of welded joint of A6N01S-T5 aluminum alloy of high-speed trains. Tensile strength and hardness changed after corrosion was tested. The micro morphologies were observed by metalloscope and laser confocal scanning microscope (LCSM). The corrosion loss and corrosion loss ratio were also investigated. The results showed that the heat affected zone (HAZ) was the most sensitive to corrosion in welded joint in the salt fog corrosion test. The potential of the corrosion of the intermetallic compound on the surface was different from the Al matrix potential, which easily generated corrosion micro-batteries that generated the corrosion pit. The weld zone was the most sensitive to corrosion in the welded joint in the intergranular corrosion test, because much corrosion produced an intermetallic phase such as $CuAl_2$, MgZn2, Mg_5Al_8, which formed the deficient Cu or Mg zone potential. The potential is low, which acted as an anode and corroded. The residual stress test on the weld of the A6N01S-T5 of the W1 of the exterior surface of roof of high speed train showed there was distributed high tensile stress and compressed stress in the weld zone, HAZ zone and matrix zone. The defects will spread under the high stress and make the corrosion become severe.

Keywords: High speed trains; Salt fog corrosion; Intergranular corrosion; A6N01S-T5 aluminum alloy; Residual stress

1. Introduction

A6N01S-T5 aluminum alloy is employed more and more in high-speed train bodies and welding structures, such as side walls, roofs and underframes. Because the A6N01S-T5 aluminum alloy is the Al-Mg-Si series alloy, it has medium strength, good extrusion, and good anti-corrosion and welding properties. Its minimum section thickness is 2.5 mm [1].

In recent years there have been many reports about the corrosion behavior of welded joints of different series of aluminum alloy [2-4]. Gong [5] studied the intergranular corrosion of 6005A aluminum alloy, and the result showed that the welding seam zone was more easily corroded than the matrix zone. Zupanc et al. [6] studied the effect of pitting corrosion on fatigue performance of shot-peened aluminum alloy 7075-T651. They proved that the corrosion occurred mainly in the heat affected zone (HAZ) of AA7075-T651 and AA7075-T6 welded joint. Jariyaboon et al. [7] studied the effect of welding parameters on the corrosion behavior of friction stir welded AA2024–T351. The results showed that the corrosion performance of the welding seam of AA2024-T3 and AA2129 welded joint was the same as that of the matrix. Wadeson et al. [8] studied the corrosion behavior of AA7108-T79 welded joint by friction stir welding and found that the partly recrystallized zone was very easily corroded.

The high speed train is constantly running under many different environments in China. It is influenced by corrosion from seawater, wind and dust, which will affect its safety.

Hence, this paper focused on the salt corrosion mechanism and intergranular mechanism of A6N01S-T5 welded joints of the high speed train.

2. Experimentation

2.1 Materials

A6N01S sample sheet is 12 mm thick with heat treatment of T5 (materials are cooled from an elevated-temperature shaping process and then artificially aged according to ISO 2107:2007). Welded joint samples were made by Metal Inert-gas (MIG) welding method (PHOENIX welding machine) with ER5356 welding wire. The chemical contents of the matrix and welding wire are listed in Table 1, the mechanical properties of A6N01S-T5 are listed in Table 2, and the weld-

*Corresponding author. Tel.: +86 28 87600625, Fax.: +86 28 87600625
E-mail address: nhuang@263.net,15816314@qq.com
† Recommended by Editor Jai Hak Park.

Table 1. Chemical composition of A6N01S-T5 matrix and ER5356 welding wire (mass percentage %).

Element	Zn	Mg	Cu	Mn	Cr	Ti	Si	others
Matrix	0.25	0.4-0.8	0.35	0.5	0.3	0.1	0.4-0.9	0.15
ER5356	0.1	4.5-5.5	0.1	0.05-0.2	0.05	0.2	0.25	-

Table 2. Mechanical properties of A6N01S-T5.

Materials	Elastic modulus (GPa)	Poisson's ratio	Yield limit (MPa)		Fatigue limit (MPa)	
			Matrix	Weld	Matrix	Weld
A6N01S-T5	69	0.3	205	120	78	39

The mechanical properties of A6N01S-T5 are according JIS 4100 H 4100-2006.

Table 3. Welding process parameters of A6N01S-T5.

Peak current (A)	Voltage (V)	Welding speed(cm/min)	Gas flow(L/min)	Welding wire diameter(mm)
230-280	24-30	35-45	25	1.6

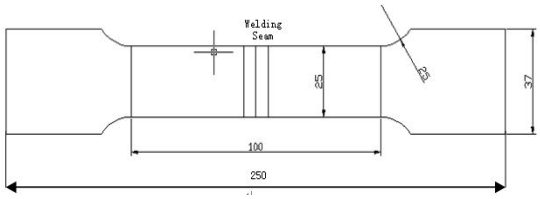

Fig. 1. Schematic diagram of sample for tensile strength test (unit: mm).

ing process parameters are listed in Table 3. Samples for tensile strength test were machined from the welded sheet, and the sample dimensions are shown in Fig. 1; the dimension of the sample is according ISO 2107:2007.

2.2 Salt fog corrosion test

Samples were cleaned by acetone, eroded in 10% NaOH solution for 10 minutes, and immersed into HNO_3 to get a shining surface. After cleaning and drying, samples were placed into salt fog cabinet (SO_2/Q-0250) with 30° angle between the test surface and vertical direction. Corrosion medium was 5% NaCl solution with $CuCl_2$ (0.26±0.02g/L), and continuous salt fog test was employed. The test time is 8 hours, 24 hours and 72 hours respectively.

2.3 Intergranular corrosion test

The matrix samples and welding joint samples were machined as 40×25×b (mm), (b: thickness<10 mm). After cleaning by acetone, eroding by 10% NaOH solution and HNO_3 to get shinning surface, samples were immersed into intergranular corrosion media which contained NaCl (1 mol·L^{-1}) and H_2O_2 (1.1 g·mL^{-1}). Test temperature was kept at 35±1°C, and test time was 16h, 48h, 64h, respectively. Corrosion products were cleaned before further testing.

2.4 Hardness test

The experiment was stopped at the preset time. After the sample was cleaned by distilled water and dried, the hardness was tested on Vicker Hardness (HV-10B) from the edge of the weld. The load was 98N and lasted for 10s.

2.5 Tensile strength test

The tensile strength test was conducted at a loading ratio of 1 mm/min on a WDW3100 electronic universal testing machine.

2.6 Microscopy observation

The morphology of samples before and after corrosion was examined by GX40-001110 metalloscope; the morphology after corrosion for 24h was observed by VK-9700K LCSM.

2.7 Corrosion ratio test

Standard solution with concentration of 0.02~0.4 μg·mL^{-1} was prepared by $KAl(SO_4)_2 \cdot 12H_2O$ (AR). HAc-NaAc buffer (pH 5.5), chrome-azurol S (CAS) solution (0.1%) and cetyltrimethylammonium bromide solution (CTMAB, 2.5 g·L^{-1}) were added into the standard solution for color reaction. The absorbance was tested at 400~800 nm with UV-visible spectrophotometer (UV-2450) to plot the absorption curve, and then the standard curve was tested at the maximum absorption wavelength. The precipitate in corrosion media was dissolved with HCl solution (1:1), and ascorbic acid solution was added to eliminate the interference of Cu and Mn; then the media was adjusted to neutral and diluted. Chromogenic reagents were added into the media and absorbance was tested at the maximum wavelength. The concentration of Al was calculated from the standard curve and the corrosion ratios of different samples were compared.

3. Results and discussion

3.1 Metallographic analysis of welded joint

The morphology of A6N01S-T5 welded joint is shown in Fig. 2. The matrix of A6N01S-T5 had flat grains with obviously rolling direction; the grain boundary is clear with some strengthening phases and irregular black inclusion phases separated out of the matrix. The grains of the HAZ zone are coarsening and the grain boundary is fuzzy and narrow; the strengthening phase Mg_2Si (black dot scope) was separated out of the HAZ zone and the inclusion phase is gray color bulk substance. The right of the fusion area is welded, and the microstructure of the weld is arborization, which is distributed on the matrix α(Al).

Table 4. Fitted data of corrosion weight loss.

	a	b	R^2	ab
6B	2.8492	0.0235	0.9785	0.066956
6W	4.1229	0.0184	0.9771	0.075861

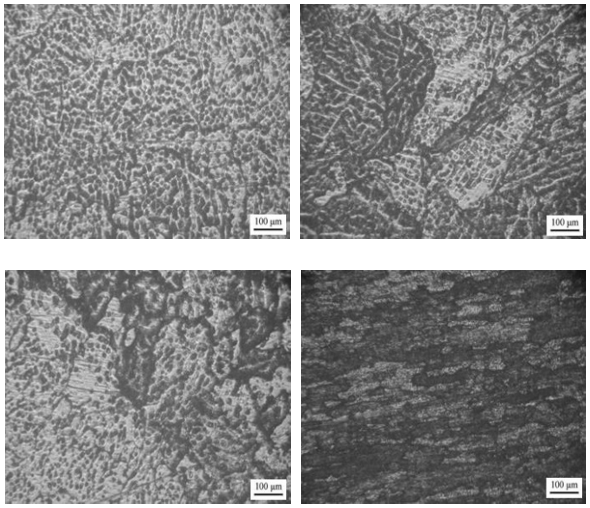

Fig. 2. Morphology of A6N01S-T5 welded joint: (a) Weld zone; (b) HAZ zone; (c) Fusion zone; (d) Matrix zone.

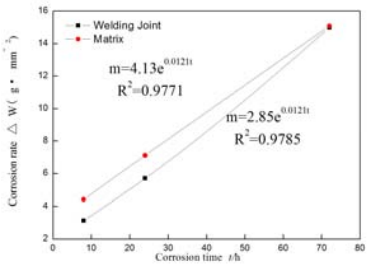

Fig. 3. Fitted curves of corrosion loss after salt fog corrosion.

3.2 Corrosion loss after salt fog corrosion

Fig. 3 is the fitted curves of corrosion loss after salt fog corrosion. Table 4 is the fitted data. The R^2 of the matrix and weld is above 0.93, and the correlation is good. The curve fit method is $m=ae^{bt}$; then by calculation we can derive the corrosion ratio V: with increase in factor ab, the corrosion ratio V goes up.

3.3 Change of hardness and tensile strength of welded joint after salt fog corrosion

The hardness of the matrix zone, HAZ and weld decreased after corrosion (Fig. 4(a)). The weld hardness decreased rapidly after corrosion, and the hardness of HAZ decreased with corrosion time. After corrosion for 72h the decrease of hardness was very obvious. From the data it was known that HAZ was the most sensitive to corrosion in the welded joint.

The tensile strength of welded joints of 0h, 8h, 24h, 72h were 122.7 MPa, 114.1 MPa, 89.9 MPa and 77.9 MPa, respectively. The tensile strength of welded joints decreased with corrosion time elapsing (Fig. 4(b)), which showed the plasticity decreasing of the welded joints. The strength decrease was rapid in the early stage and slowed down after 24h. The points of tensile fracture were at the weld junction, which showed that HAZ has the lowest strength.

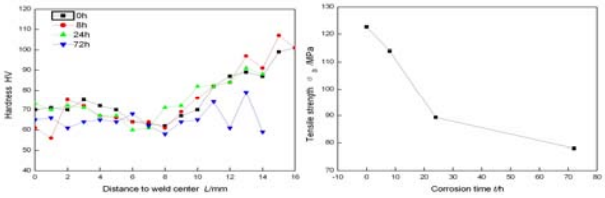

(a) (b)

Fig. 4. Hardness change (a) and tensile strength change (b) of A6N01S-T5welded joints after different corrosion periods.

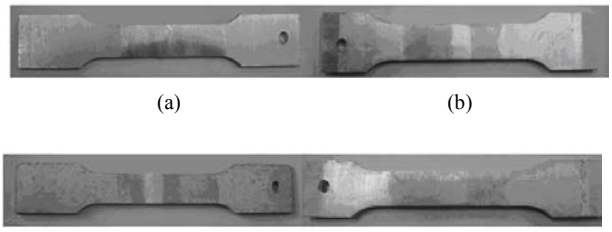

(a) (b)

(c) (d)

Fig. 5. Photos of samples after corrosion for (a) 0h; (b) 8h; (c) 24h; (d) 72h.

3.4 Morphology of welded joint after salt fog corrosion

The photos of welded joints before and after corrosion are shown in Figs. 5 and 6. There are obvious corrosion products distributed on the surface of the HAZ zone. Over time, the weld surface stayed relatively bright with a few distributed corrosion spots.

On the surface of the HAZ zone, the corrosion spots distributed more densely and became bigger after 72h.

The surface of matrix and weld after 24h test was magnified to 1000 times and 3000 times respectively by LCSM (Fig. 7).

The corrosion pit could be seen after 24h for the matrix; the corrosion cracks spread along the grains boundaries (Fig. 7(c)). The maximum depth of corrosion pit was 5.8 μm, and the area ratio of the corrosion was 2.56%. Corrosion products covered the weld after 24h, and the corrosion cracks spread along the grain boundaries (Fig. 7(e)); the maximum depth of corrosion pit was 6.5 μm, and the area ratio of the corrosion was 22.84%. It can be concluded that the corrosion extent of the weld is more severe than the matrix.

Because the potential of the corrosion of the intermetallic compound on the surface is different from the Al matrix potential, it is easy to generate a corrosion micro-battery. When the corrosion potential of the second phase is the negative on the Al matrix (η phase or S phase), the second phase first dissolves in the solution and generates the corrosion pit. When

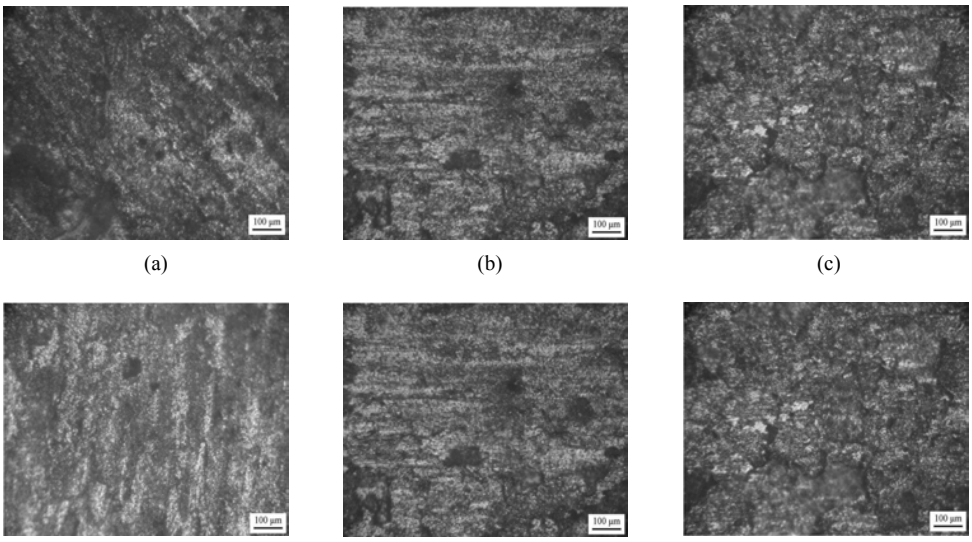

Fig. 6. Micro-morphology of HAZ zone after corrosion for (a) 8h; (b) 24h; (c) 72h and weld after corrosion for (d) 8h (e) 24h (f) 72h.

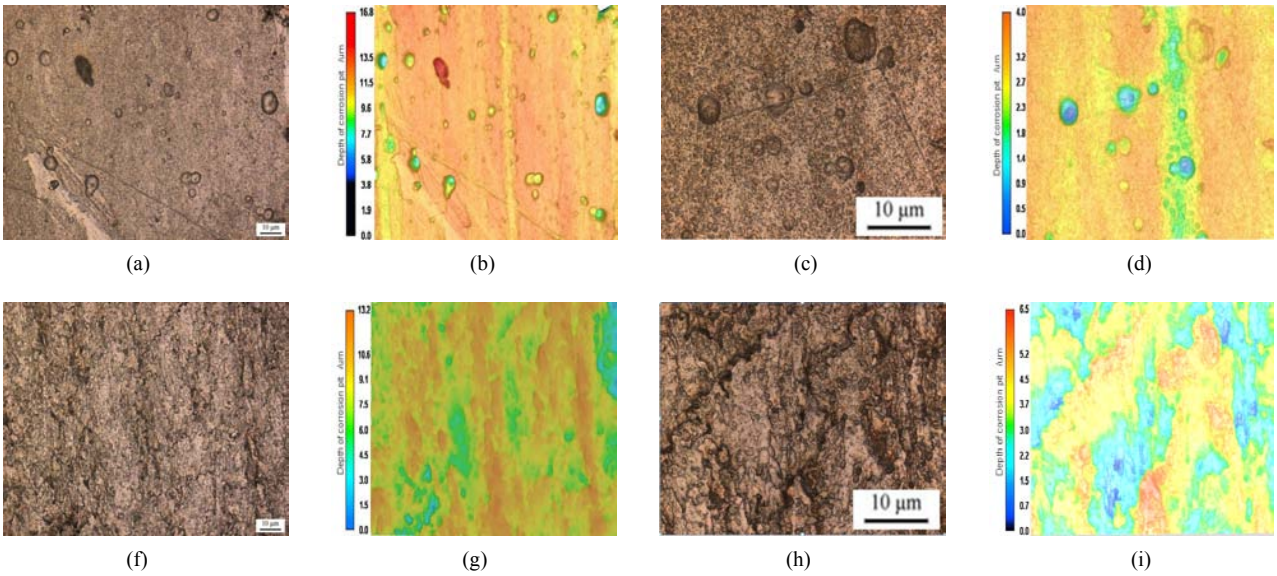

Fig. 7. LCSM morphology of matrix: (a) ×1000; (b) 2D image ×1000; (c)×3000; (d) 2D image ×3000 and weld; (e)×1000; (f) 2D image ×1000; (g)×3000; (h) 2D image ×3000 after corrosion for 24h.

the corrosion potential of the second phase is the positive on the Al matrix $(Al,Cu)_6(Fe,Cu)$,Al_7Cu_2Fe phase), the Al matrix first dissolves in the solution, which makes the second phase break off the surface and it generates the corrosion pit.

The pit corrosion of the Al alloy and the accumulation of the corrosion products provide the attachment point of the spread to the Al alloy surface for the oxygen ion. The corrosion medium is easy to penetrate through the Al alloy matrix and generates a chemical reaction with the Al alloy. The corrosion solution is easy to generate an attachment point in the corrosion pit too. The corrosion reacts with the Al completely, the local corrosion becomes severe.

Fig. 8 is the absorption curve of Al^{3+} and standard curve. Fig. 9 is the Al content of matrix and welding joint in corrosion media. The reaction of Al^{3+} with CAS and CTMAB in HAc-NaAc buffer with appropriate PH value will produce a blue ternary complex. From the absorption curve the maximum absorption was found at 617 nm (Fig. 8(a)). The standard curve showed a good linear relationship in accordance with Lambert-Beer's Law in 0~0.4 $ug{\cdot}mL^{-1}$ (Fig. 8(b)). The corrosion media was measured and Al^{3+} concentration was fitted with the exponent curve (Fig. 9). It was found that Al^{3+} concentration increased as corrosion time increased for all samples, and the concentration of 6W was higher than that of 6B at each time point. Cl^- in the corrosion media was a key factor for A6N01S-T5 Al-alloy to be corroded which sub-

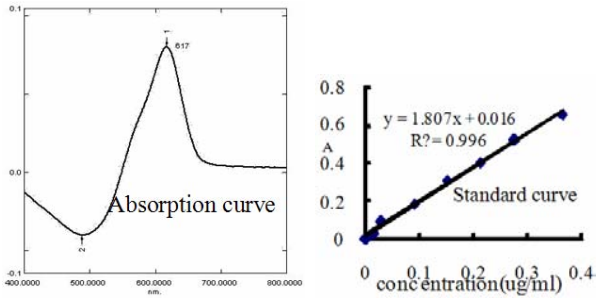

(a) (b)

Fig. 8. Absorption curve of Al^{3+} (a) and standard curve (b).

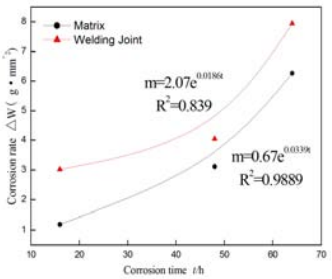

Fig. 9. Al content of matrix and welding joint in corrosion media.

stituted OH^- of oxide membrane on the sample surface through competitive absorption, and led to Al dissolving into the media by the form of water-soluble $AlCl_3$. The higher concentration of Al^{3+} in media meant a higher corrosion ratio of the sample.

3.5 Corrosion loss after intergranular corrosion

Fig. 10 is the fitted curves of corrosion loss after intergranular corrosion. Fig. 11 is the LCSM morphology after corrosion for 64h. The intergranular corrosion occurred in the surface of the welded joints, then spread along with the inner, and the intergranular corrosion spread faster surrounding the gas hole and inclusions (the black spot in the morphology). The corrosion extent of the weld zone was more severe than the HAZ zone and the matrix zone, and the morphology of the corrosion was net-like. Because much corrosion products (e.g.$CuAl_2$, $MgZn_2$, Mg_5Al_8) were generated, there formed the deficient Cu or Mg zone potential. The potential in this zone is low, which acted as an anode and corroded.

Table 4 is the depth and area ratio of corrosion pits. The surface of the matrix zone, HAZ zone and weld zone are all affected by the corrosion. The corrosion produced exfoliation. The maximum depth of the corrosion pit was 6.25 μm and the area ratio of the corrosion was 13.3% (Fig. 11(a3)) of the matrix. The maximum depth of corrosion pit was 11.25 μm, the area ratio of the corrosion was 29.9% (Fig. 11(b3)) of the HAZ zone. The maximum depth of corrosion pit was 28μm and the area ratio of the corrosion was 35.6% (Fig. 11(c3)) of the weld zone. The severe corrosion zone was on the weld.

Fig. 12 is the residual stress results of the A6N01S-T5 of

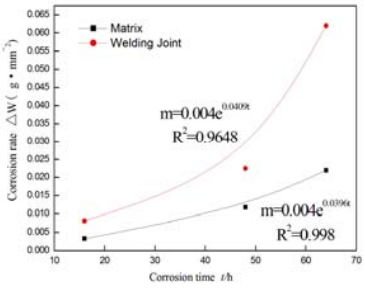

Fig. 10. Fitted curves of corrosion loss after intergranular corrosion.

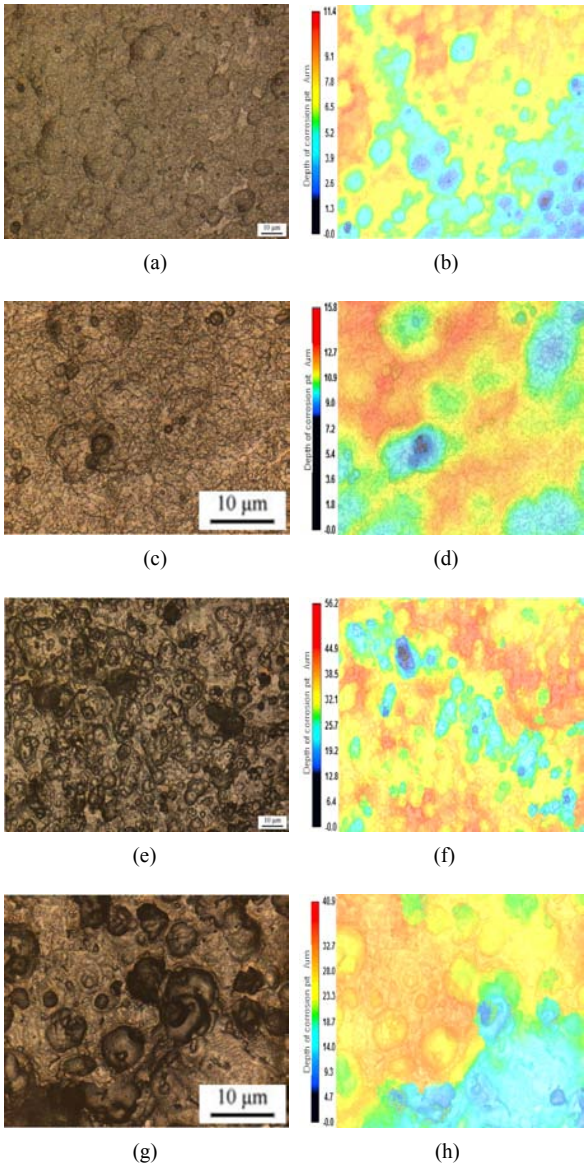

(a) (b) (c) (d) (e) (f) (g) (h)

Fig. 11. LCSM morphology Of matrix: (a) ×1000; (b) 2D image ×1000; (c) ×3000; (d) 2D image×3000 and weld; (e)×1000; (f) 2D image ×1000; (g)×3000; (h) 2D image×3000 after corrosion for 64h.

the W1 of the exterior surface of roof of high speed train. It indicates that the maximum tensile stress was approximately 157.3 MPa, which was near the yield strength of the A6N01S-

Table 5. Depth and area ratio of corrosion pits.

	Depth(μm)	Area ratio (%)
Matrix	6.25 ± 0.5	13.3
HAZ	11.25 ± 2.1	29.9
Weld	28 ± 7.1	35.6

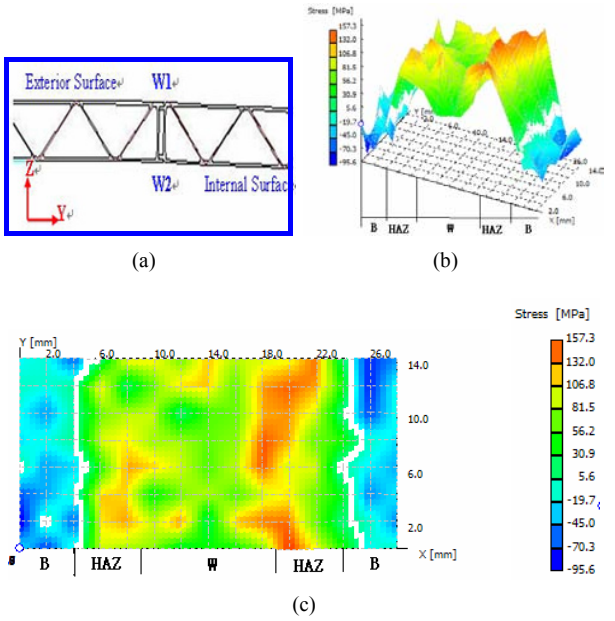

Fig. 12. The residual stress results of the A6N01S-T5 of theW1of the exterior surface of roof of high speed train.

T5 alloy. It can be concluded that if there are corrosion products distributed on the surface of the welded joints, there may be cracks, pores and other defects. The cracks and other defects will spread under high stress and then make the corrosion more severe.

4. Conclusion

The salt fog corrosion test showed that the most sensitive zone is the HAZ zone. The corrosion mechanism is based on the potential of the corrosion of the intermetallic compound on the surface being different from the Al matrix potential. This generated corrosion which in turn caused micro-battery and then generated, the corrosion pit. The corrosion cracks spread along the grain boundaries. The maximum depth of corrosion pit was 6.5 μm and the area ratio of the corrosion was 22.84%.

The intergranular test showed the weld zone was sensitive to corrosion on the welded joint. The corrosion generated many products (e.g., $CuAl_2$, MgZn2, Mg_5Al_8), which led to the formation of the Cu and Mg deficit zone where the potential is low and that acts as an anode, which in turn corroded. The intergranular corrosion decreases the binding force between the grains, resulting in fracturing at the intergranular zone.

Through the residual stress test of the weld of the A6N01S-T5 of the W1 of the exterior surface of roof of high speed train, the result showed that high tensile stress and compressed stress were distributed in the weld zone, HAZ zone and matrix zone. The defects will spread under the high stress and make the corrosion became severe.

Acknowledgment

The authors are grateful to the Projects in the National Science & Technology Program (No. 2009BAG12A04).

References

[1] N. Hideo, *Innovation of railway transport and development of people's living condition-the Japanese experience*, China Railway Publishing House, Beijing, China (2002).

[2] C. S. Paglia and R. G. Buchheit, A look in the corrosion of aluminum alloy friction stir welds, *Scripta Materialia*, 58 (6) (2008) 383-387.

[3] A. Raman and B. Kuban, The application of infrared spectroscopy to the study of atmospheric rust systems-I Standard spectra and illustrative applications to identify rust phases in natural atmospheric corrosion products, *Corrosion Science*, 32 (12) (1991) 1295-1306.

[4] C. P. Chan and T. M. Yue, The effect of excimer laser surface treatment on pitting corrosion fatigue behavior of aluminum alloy 7075, *Journal of Materials Science*, 38 (7) (2003) 2689-2702.

[5] F. T. Gong and C. J. Fu, The corrosion behavior of A6005A aluminum alloy welding joints, *Journal of Dalian Jiaotong University*, 30 (5) (2009) 67.

[6] U. Zupanc and J. Grum, The effect of pitting corrosion on fatigue performance of shot-peened aluminum alloy 7075-T651, *Journal of Material Processing*, 210 (2) (2010) 1197.

[7] M. Jariyaboon and A. J. Davenport, The effect of welding parameters on the corrosion behavior of friction stir welded AA2024–T351, *Corrosion Science*, 49 (4) (2007) 877.

[8] D. A. Wadeson, X. Zhou and G. E. Thompson et al., Corrosion behavior of friction stir welded AA7108 T79 aluminum alloy, *Corrosion Science*, 48 (3) (2006) 887-897.

Guo-qing Gou is a lecturer at the School of Materials Science and Engineering, Southwest Jiaotong University (SWJTU), China. His research interest is welding technology and non-destructive testing. At least 20 of his papers have already been published.

Nan Huang is a professor and Ph.D supervisor at the School of Materials Science and Engineering, Southwest Jiaotong University (SWJTU), China. His research interest is coating technology and materials protection. At least 100 of his papers have already been published.